CrossMark

ORIGINAL ARTICLE

Novel approach towards finite element analysis of residual stresses in electrical discharge machining process

Mohammadreza Shabgard[1] · Soleyman Seydi[1] · Mirsadegh Seyedzavvar[1]

Abstract The high temperature gradients generated in electrical discharge machining process by electric discharges result in residual stresses on the surface layers of electrodes. These residual stresses can lead to deficiencies in machined workpiece such as micro-cracks, reduction in strength and fatigue life, and possibly catastrophic failure. In the present research, a finite element model (FEM) has been developed to estimate the distribution of residual stress in the machined surface of workpiece through considering temperature-dependency of the physical properties of AISI H13 tool steel as workpiece and solid-state phase transformation. The data achieved by FE simulation have been validated using experiments handled by nano-indentation measurement on the side of cubic ED-machined workpiece. The results showed that the profile form of residual stress is independent from discharge energy; though with increase in pulse energy, the maximum of tensile residual stress and the depth where the maximum is observed slightly increase. Furthermore, the maximum calculated value for residual stress exceeds ultimate strength of AISI H13 tool steel, 1990 MPa, and reaches the amount of 2150 MPa for lowest pulse energy. The maximum residual stress measured by nano-indentation is 2040 which represents the slight deviation of 50 MPa or 2.5 % with the predicted values.

✉ Mohammadreza Shabgard
mrshabgard@tabrizu.ac.ir

[1] Department of Manufacture, Faculty of Mechanical Engineering, University of Tabriz, Tabriz, Iran

1 Introduction

Electric discharge machining (EDM) is a thermal process where thermal energy is generated in a discharge channel, called plasma channel. Extremely high temperature resulted from the transient heat flux, induces thermal and consequently residual stresses within the surface layers of the workpiece. These residual stresses can lead to defects in the machined workpiece such as micro-cracks, decrease in strength and fatigue life, and possibly catastrophic failure. Thus, it is of paramount importance to develop methods of predicting the settings of machining in which the level of residual stresses exceeds over the permissible values [1, 2].

Phase transformation from solid to liquid as well as liquid to vapor occurs during the heating cycle of every discharge. Part of the transformed material is removed but the rest re-solidifies on the surface of the workpiece. This re-solidified layer is usually called the white layer, as it is not easily etchable. Below the re-solidified white layer lies a second layer that does not melt but is still affected by heat. For steels, during the cool-down cycle, solid-state transformations occur in this heat-affected zone because the highest temperature reaches beyond the austenite transformation temperature [3]. Mamalis et al. [4] with some micro-hardness and micrograph measurements have shown that most of the heat-affected zone transforms to martensite.

A lot of efforts have been made to introduce numerical models for EDM process in order to predict temperature distribution during each electric discharge and thereafter estimate the profile and size of crater formed by every single discharge, the material removal rate (MRR), and the tool wear rate (TWR). In the late 80s, DiBitonto et al. [5, 6] developed a model based on point heat source for cathode erosion of EDM process and disk-shaped heat source with Gaussian distribution of heat flux for anode erosion, and compared them

🖄 Springer

with their experimental studies. These works were considered as bench mark in the modeling of EDM process. Joshi and Pande [7] have developed a comprehensive thermal model of EDM process using finite element method. They have incorporated important factors such as the Gaussian distribution of heat flux, and EDM spark radius as a function of discharge current and discharge duration. These considerations have greatly improved accuracy of prediction and made the introduced model closely comparable to the actual process conditions. Tan and Yeo [8] conducted a numerical modeling study based on finite element method using multi-discharge approach to elucidate the physics and characteristics of powder-mixed micro EDM process. They considered the presence of powders in the gap distance into account by an estimated factor of 1.07 for heat source expansion at powder concentration of 0.02 g/L. The authors employed ANSYS software for their objectives and considered the thermo-physical properties of electrode material independent from temperature. They reported that their model provides acceptable predictions of the process performance measures, including R_{max} and recast layer thickness, although further refinements are required to acquire results with better accuracy. Shen et al. [9] studied the energy distribution during the EDM process of Ti-6Al-4 V alloy. In their model, the energy distribution and plasma channel diameter were determined though comparing the boundary of melted material in the crater acquired by metallurgical observations and isothermal profile of thermal-physical model calculated through finite element simulation and via assuming constant plasma diameter and energy distribution into workpiece. The authors iterated this procedure until the calculated and measured boundaries coincided. Residual stresses induced into the surface layers of workpiece by the EDM process are the product of extreme temperature gradient and localized inhomogeneous plastic deformation due to metallurgical transformations in the locality of electric discharges [10]. Recently, few numerical studies have performed to simulate the thermal and residual stresses induced in the surface layers of electrodes due to temperature gradient caused by the electric discharges. Yadav et al. [1] have developed a finite element model to estimate the temperature field and thermal stresses due to Gaussian distributed heat flux of a spark during EDM in HSS workpiece. They observed that after each spark, substantial compressive and tensile stresses develop in a thin layer around the spark location that exceed the yield strength of the workpiece mainly in an extremely thin zone near the spark location. Yeo and Murali [11] have developed a mathematical model based on heat transfer principles for the simulation of single-spark machining during micro-electro discharge machining (μEDM) of Ti–6Al–4V titanium alloy. Simulated crater dimensions and residual stresses were compared with experimentally observations acquired using atomic force microscope (AFM) and a nano-indentation technique. They report that the residual

stress exceeded the ultimate tensile strength (860 MPa) of the material near the center of spark location and gradually subsided by the distance from the center. Das et al. [12] have presented a finite element-based model in the form of a commercial software called DEFORM for the electric discharge machining process. The model used process parameters such as power input, pulse duration, etc. to predict the transient temperature distribution, liquid and solid-state material transformation, and residual stresses that are induced in the workpiece as a result of a single discharge. An attractive feature of the model is its ability to predict the shape of the crater that is formed as a result of material removal. Rebelo et al. [13] have made a finite element model (FEM) based on an individual discharge to calculate the residual stresses originating from EDM with different discharge energies. The model used axi-symmetric elements and the temperature-dependent thermo-mechanical properties of stainless steel AISI 304. The calculated residual stress profiles were in good agreement with experimental results. Ekmekci [14] simulated the residual stress distribution in EDM process with finite element method using commercial software called ANSYS. In another attempt, Ekmekci et al. [15] experimentally investigated residual stress profiles using layer removal method. They utilized electrochemical machining and recoded the corresponding deformations due to stress relaxation by removal of layers and employed elasticity theories in order to acquire the stress profiles. From these experiments, they presented a semi-empirical approach for estimating residual stress profiles along the depth in different pulse currents and pulse durations, and concluded that maximum value of tensile residual stresses is about the ultimate tensile strength of the material and unchanged with respect to spark energy. Predhan [16] simulated the stress state in AISI D2 steel machined by EDM process using finite element commercial code ANSYS. The author in his models presented the effect of discharge current and duration on temperature distribution and thermal stresses in the surface of work electrode. He reported that the thermal stresses affect to a larger depth of ED-machined surface as pulse energy increases.

In the present work, in order to predict the distribution of residual stresses in workpiece due to EDM process, a model has been developed based on a sequentially coupled thermal, metallurgical, mechanical 3-D finite element method. In this model, effects of volume change due to austenite–martensite transformation on the final residual stress, or in other words, solid-state phase transformation in the estimation of the residual stress distribution, has been taken into account. The commercial finite element solver ABAQUS code has been employed in the simulation stages. ABAQUS code allows us to consider the time dependency of heat flux growth over the surface of part domain and also heat dependency of physical properties of work material in our simulations. A nano-indentation technique has been used in experiments in order to

validate the results of numerical simulations. The objectives of our attempt was set to develop a reliably sufficient model to estimate the range of input parameters in order to reach the lower levels of induced stresses at the surface of ED-machined surface and reduce the probability of occurring problems, such as micro-cracks, associated with it. Also, this work is aimed to provide better inside into the physics behind the stress developing mechanism in work material processed by EDM through a more realistic simulation of thermo-physical phenomenon during the electric discharges.

2 Finite element modeling of EDM process

Extreme temperature gradient in EDM process in the locality of each discharge causes non-uniform local expansion of workpiece material being restrained which leads to high residual stresses induced into the surface layers of workpiece. In this study, in order to determine the induced stress in the workpiece, a sequentially coupled thermal, metallurgical, mechanical 3-D finite element model is developed based on ABAQUS code. Effects of volume change due to austenite–martensite transformation on the final residual stress are considered. The solution procedure consists of two steps; first, the temperature distribution and its history in the EDM model are computed by the transient thermal analysis. Then, the temperature history is employed as a thermal load in the subsequent mechanical elastic–plastic calculation of the residual stress field. In this step, the volume fraction of martensite is also calculated, and volume change due to phase transformation is considered through modifying the thermal expansion coefficient over the temperature range in which austenite changes into martensite. A small cubic portion of the workpiece around the spark as shown in Fig. 1 is taken as the domain.

Because of the symmetry, only one-quarter of the domain is considered into account during the analyses. The

Fig. 1 Thermal model of EDM process. Γ_2 and Γ_5 are planes of symmetry and heat flux applied on Γ_1

following assumptions are made due to the random and complex nature of EDM.

1. The domain is considered as symmetric.
2. The workpiece material is homogeneous and isotropic.
3. The material properties for the workpiece are temperature dependent.
4. Heat transfer is through conduction within the workpiece and convection at the workpiece-dielectric liquid interface, respectively.
5. The workpiece is assumed as stress-free before EDM.
6. The workpiece material is elastic-perfectly plastic and yield stress in tension is the same as that in compression.
7. The analyses are handled for single spark.

2.1 Thermal analysis

The cubic portion of the workpiece around the spark struck location has been considered as semi-infinite solid. In the Fig. 1, the schematic of heat transfer model and applied boundary conditions are shown. In Cartesian coordinate, the following three-dimensional transient heat transfer equation has been solved [11]:

$$\rho C \frac{\partial T}{\partial T} = Q + \frac{\partial (k_x \partial T/\partial x)}{\partial x} + \frac{\partial (k_y \partial T/\partial y)}{\partial y} + \frac{\partial (k_z \partial T/\partial z)}{\partial z} \quad (1)$$

where the temperature T is a function of the position and time, k_x and k_y and k_z are the thermal conductivity, ρ is the density and C is the specific heat of the workpiece, and Q is the energy transferred to the workpiece.

$$
\left.
\begin{array}{l}
k \dfrac{\partial T}{\partial y} = h_C (T - T_0) \qquad\qquad \text{for spark off-time} \\[2mm]
\left.
\begin{array}{ll}
k \dfrac{\partial T}{\partial y} = q_w & \text{if } r \le R(t) \\[2mm]
k \dfrac{\partial T}{\partial y} = h_C (T - T_0) & \text{if } r > R_{(t)}
\end{array}
\right\} \text{ for spark on-time}
\end{array}
\right\} \text{ on } \Gamma_1
$$

$$(2)$$

$$k \frac{\partial T}{\partial x} = k \frac{\partial T}{\partial y} = k \frac{\partial T}{\partial z} = 0 \quad \text{on } \Gamma_2 - \Gamma_4, \Gamma_5, \text{ and } \Gamma_6 \quad (3)$$

where q_w is the quantity of heat flux entering into the workpiece, $R(t)$ is the radius of spark at each time, h_c is the heat transfer coefficient, and T_0 is the ambient temperature. During the spark, on-time energy is transferred to the workpiece through top surface Γ_1 as heat flux and during the spark off-time heat is lost from the very same surface of workpiece to the dielectric liquid. This condition is modeled using the convective heat transfer. The temperature-dependent convection coefficient of the dielectric oil is given in Table 1.

The boundaries Γ_4, Γ_3, and Γ_6 are far distant from the input heat flux that there is no heat transfer across them. And on the
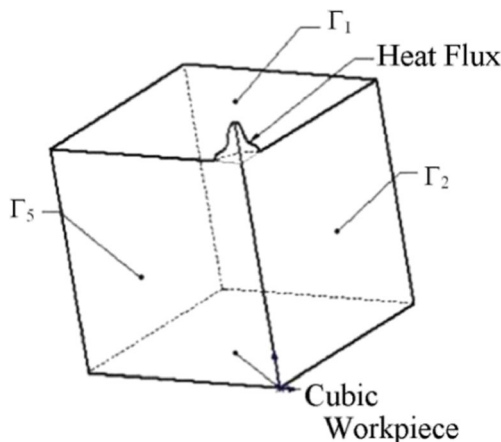
Table 1 Temperature-dependent convection coefficient of the dielectric oil (W/m² K) [13]

Temperature (°C)	20	200	600	720
Convection coefficient of the dielectric oil (W/m² K)	668.9	668.9	3177	836.2

two planes of symmetry Γ_2 and Γ_5, adiabatic boundary conditions are dominant.

Important factors which contribute to the accurate prediction of the thermal history after every single discharge in heat transfer model of EDM process include the fraction of produced heat in plasma channel transferred to the workpiece, radius of plasma channel, and the thermo-physical properties of material. In this work, the Gaussian distribution has been employed as input heat flux in the modeling stage of thermal distribution into workpiece. Eq. (4) represents this model [1].

$$q_w(r) = \frac{4.45 F_c U_b I}{\pi R^2(t)} exp\left\{-4.5\left(\frac{r}{R(t)}\right)^2\right\} \quad (4)$$

where U_b is discharge voltage, I is current, F_c is the fraction of total spark energy transferred to the cathode, and $R_{(t)}$ is the spark radius at the workpiece surface.

Spark radius is an important factor in the modeling of EDM process. Ikai and Hashiguchi [17] have derived a semi-empirical equation of spark radius namely "equivalent heat input radius" as a function of discharge current (I) and spark on time (T_{on}), which is more realistic as compared to other approaches. The following equation represents this function:

$$R_{(t)} = (2.04e-3)I^{0.43}T_{on}^{0.44} \quad (5)$$

Energy distribution factor is another important item in the thermal analysis of EDM process. The total thermal energy due to spark gets divided into three parts; one portion is conducted away by the cathode and the other by the anode, and the rest dissipates into the dielectric. DiBitonto et al. [5, 6] conducted their experimental and analytical studies over a variety of operational conditions with considering the energy distribution for cathode (F_c) equal to 0.183. The data achieved by their analytical models corresponds directly to the experimental results with a high degree of accuracy. In the present work, the same value of F_c (0.183) has been utilized in simulation procedures.

2.2 Solid-state phase transformation

Thermal cycles during the EDM process are responsible for the solid-state phase transformation in the workpiece material which results in volumetric changes and subsequent residual stresses in the machined workpiece. The solid-state phase transformation often plays a dominant role in the modeling

of thermo-mechanical problems. When AISI H13 tool steel is heated over A_1 (cementite disappearance temperature) temperature during the heating phase of EDM process, the microstructure of parent material starts to transform into austenite, and when the temperature reaches A_3(ferrite disappearance temperature), pearlite, ferrite, and martensite completely changes into austenite. Subsequently, as the austenite cools during the cooling stage after each discharge, several daughter phases, such as ferrite, pearlite, or bainite could be transformed from austenit. These solid-state transformations are controlled by the cooling rate of the transformed austenite and the composition of the parent material. As the cooling rate increases, the tendency to the formation of martensite intensifies. Since the cooling rate in EDM process is extremely high, it is expected that most of the heat-affected zone to be transformed to martensite [12]. The results of the metallurgical studies conducted by Mamalis et al. [4] corroborate this phenomenon.

During rapid cooling, austenite begins to transform into martensite with a body centered tetragonal (b.c.t.) structure, thus the volume increases. The volume change due to phase transformation during heating and cooling is schematically shown in Fig. 2.

In the present model, at first, based on the thermal analysis results, the extent of the fusion zone (i.e., the re-solidified molten layer) and the heat-affected zone, that mostly contains martensitic material, has been predicted. Nodal temperature data from the heat transfer analysis determines the region that melts and the region that experiences temperature above the A_3 but still stays below the fusion temperature. Later, in order to consider the removed material due to EDM process, some of the fusion reign elements were removed with 'model change' feature of ABAQUS code. The rest of elements solidified to form the fusion zone (white layer on the surface of the workpiece).
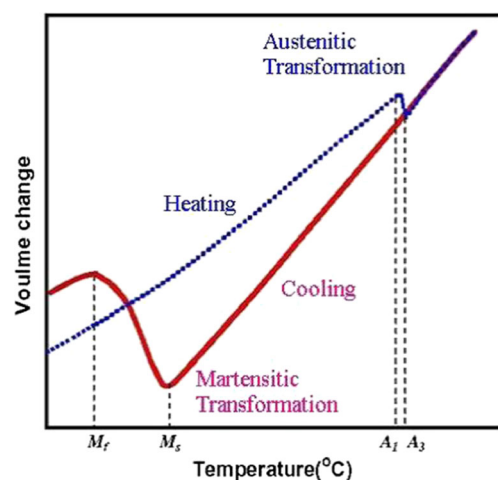

Fig. 2 Schematic diagram of volume change due to phase transformation [18]

There have been several studies concerning the amount of molten material that removed at the end of heating phase. DiBitonto et al. [5, 6] defined a factor called plasma flushing efficiency (PFE) as the ratio of the actual volume of the material removed to the total volume of the theoretically predicted molten pool. They showed that the PFEs increase with the increase in current and pulse time. Low energy plasma fails to build enough pressure to expel a significant amount of molten material by the collapse of plasma channel at the end of discharge, whereas for high-energy content plasma, PFE is very high.

Due to the high cooling rate, the dominant phase due to solid-state transformation is martensite. As a result, all the heat-affected zone is considered to transform into martensite and the martensite fraction factor is assumed to be 1.

2.3 Mechanical analysis

The same FE mesh as in the thermal analysis was used in the mechanical analysis, except for the element type and different boundary conditions. The analysis is based on the temperature history calculated in the thermal analysis which represents the input information of subsequent mechanical analysis. The movement in the axial and the x direction of the bottom surface of cubic model (Γ_6), and the z direction of Γ_3 surface of symmetry was restrained in order to appropriate the model of actual EDM machining conditions. Temperature dependency of material properties, as shown in Table 2, was taken into account.

The high thermal gradients created during the electric discharge causes considerable local thermal expansions of the workpiece material that themselves lead to high thermal and residual stresses. The distribution of thermal and residual stresses due to thermal loading can be expressed as:

$$\{\sigma\} = [D](\{\varepsilon\} - \{m\}) \tag{6}$$

where $[D]$ is the elasticity matrix, $\{\sigma\}$ is the stress vector, $\{\varepsilon\}$ is the mechanical strain vector, and $\{m\}$ is the thermal strains vector [1].

Along with the thermal strain, an additional strain is induced by microstructural evolution during solid-state phase transformation during the EDM process. Therefore, the strain increment can be written as follows:

$$\Delta\varepsilon = \Delta\varepsilon^\varepsilon + \Delta\varepsilon^P + \Delta\varepsilon^T + \Delta\varepsilon^{\Delta V} \tag{7}$$

The various components in this equation represent strains due to elastic, plastic, and thermal loading, and the component $\Delta\varepsilon^{\Delta V}$ is caused by volume change due to phase transformation, respectively [1].

As mentioned previously, formation of martensite is accompanied by volume increase and this gives rise to internal resisting stresses [20]. The strain due to volume change associated with full martensitic transformation for high carbon steel which is used in this work is $\varepsilon_c^{\Delta V*} = 7.5 \times 10^{-3}$ [21]. The volume change due to austenite transformation is assumed to be $\varepsilon_h^{\Delta V*} = 2.88 \times 10^{-3}$ [18].

The strain caused by volume change due to the formation of austenite during heating stage was also considered in the FE analysis. In order to incorporate the effects of volumetric reduction during austenitic transformation into the FE model, a simplified linear correlation for the volume change strain in heating was adopted which is presented in the following equation [22]:

$$\Delta\varepsilon_h^{\Delta V} = -\frac{\Delta T_h}{A_3 - A_1} \times \varepsilon_h^{\Delta V*} \tag{8}$$

where $\Delta\varepsilon_h^{\Delta V}$ is the volume change strain increment and ΔT_h is the temperature increment during heating.

According to the Koistinen–Marburger (K-M) relationship [22], the strain increment due to volume change in the course of the martensitic transformation process can be determined by the following equation [14]:

$$\Delta\varepsilon_c^{\Delta V} = f \times \{-0.001 \ \exp(0.011[T - M_s]\} \times \Delta T_c \times \varepsilon_c^{\Delta V*} \tag{9}$$

where f is the fraction of martensite which is assumed to be 1, M_s is martensite-start temperature, and ΔT_c is the increment of temperature during cooling.

Table 2 Temperature-dependent AISI H13 material properties used for FEM simulation [19]

Temperature (°C)	Thermal conductivity (W/mK)	Specific heat (J/kg K)	Thermal expansion coefficient (10^{-8} C^{-1})	Young's modulus (GPa)	Ultimate tensile strength (MPa)
20	27.2	560	10.9	211	1990
100	27.8	582	11.9	209	1940
200	28.4	593	12.3	206	1860
300	28.6	598	12.7	201	1820
400	29.2	601	13.0	197	1358
500	29.8	608	13.3	194	1075
600	30.3	618	13.5	190	750

In the numerical simulations, it is assumed that when the temperature cools to M_f, the martensitic transformation is finished. The initial transformation temperature M_s can be calculated using the following equation [18]:

$$M_s = 561 - 474C - 33Mn - 17Ni - 17Cr - 21Mo \tag{10}$$

For considering these volumetric changes in our FEM simulation, a subroutine to ABAQUS code was developed that accounts for volumetric changes due to temperature changes and the phase transformation.

3 Experimental procedures

3.1 Materials and ED-machining

The material used for the experiments is AISI H13 air hardening hot work tool steel. Metallurgical composition of this steel is presented in Table 3. The cubic workpiece with dimension of $12 \times 12 \times 12$ mm^3 was machined from a thick plate, ground, heated up to 600 °C for 1 h and cooled down slowly in the air, and later relieved from residual stresses prior to electrical discharge machining to ensure stress-free condition. The experiment was carried out on a RoboForm-200 EDM machine. In this study, cylindrical pure copper electrode with diameter of 19 mm is used as anode. Kerosene was used as dielectric liquid. Nano-indentation technique was used to measure the residual stress after EDM process [23]. Since in this method fine surface finish is required, mechanical grinding and polishing operation was carried out on the specimen surfaces. The other machining parameters used in this experiment are given in Table 4.

3.2 Residual stress evaluation methodology

A nondestructive nano-indentation technique was used to measure residual stresses of an EDMed workpiece. This technique is based on the key concepts that the deviatoric stress part of residual stress affects the change in indentation load-depth curve, and then by analyzing difference between residual stress-induced indentation curve and residual stress-free curve, quantitative residual stress of target region can be evaluated. The residual stress cause to change in indentation deformation: the applied load for the tensile-stressed state is lower than that for the stress-

free state for the same maximum indentation depth. In other words, the maximum indentation depth desired is reached at a smaller indentation load in a tensile-stressed state because a residual stress-induced normal load acts as an additive load to the applied load. Therefore, the residual stress can be evaluated by analyzing the residual stress-induced normal load [25, 26].

Residual stress is assumed to be equi-biaxial in-plane state ($\sigma_{res,x} = \sigma_{res,y} = \sigma_{res}$, $\sigma_{res,z} = 0$) and is separated into hydrostatic stress ($\sigma^M = 2\sigma_{res}/3$) and plastic-deformation-sensitive shear deviator stress ($\sigma_z^D = 1\sigma_{res}/3$). The stress component along the indentation axis in the deviator stress part ($\sigma_z^D = 1\sigma_{res}/3$) is directly added to the surface-normal indentation pressure. Thus, the difference in the indentation load between stressed and unstressed specimens indented to a penetration depth, $L_T - L_0$, is defined as a residual stress-induced normal load. The contribution of an equi-biaxial residual stress on the normal indentation load can be expressed as [27]:

$$\sigma_{res} = \{3(L_0 - L_T)\} / (2A_C^T) \tag{11}$$

where A_C^T is the true contact area between indenter and specimen.

Since there are complex biaxial residual stress states in actual structures, wide application of the experimental and theoretical models of indentation technique are limited. To determine the directionality and magnitude of an actual biaxial stress, we denoted one major stress component of the biaxial applied stress as $\sigma_{res,x}$ and the other as a minor stress component $\sigma_{res,y}$; $\sigma_{res,y}$ can be expressed as $k\sigma_{res,x}$ using a stress ratio k or $\sigma_{res,y}/\sigma_{res,x}$, where k ranges from -1.0 in the pure shear stress through zero in the uniaxial stress to 1.0 in the equi-biaxial stress states [27]. In this case, if the stress ratio k is already known, individual principal stress components can also be calculated from the nano-indentation test using the following equation [27]:

$$\sigma_{res,x} = \{3(L_0 - L_T)\} / \{(1 + T)A_C^T\} \tag{12}$$

Lee et al. [27] tried to estimate the stress ratio by analyzing the pile-up heights along the two principal biaxial stress axes. The ratio of stress-induced pile-up shifts was linearly proportional to the stress ratio. A non-equi-biaxial stress applied brought about different pile-up variations along two orthogonal straining axes and the asymmetric deformation behavior was related with a ratio of its two principal stress components. In this study, since AISI H13 tool steel is

Table 3 Chemical composition of H13 tool steel [24]

Elements (%)							
Element	C	Mn	Si	Cr	Ni	Mo	V
%	0.32–0.45	0.2–0.5	0.8–1.2	4.75–5.5	0.3 max	1.1–1.75	0.8–1.2

Table 4 Machining parameters used in experiment

Open voltage	Current	Pulse on-time	Pulse off-time	Workpiece polarity
200 V	4 A	100 μs	50 μs	Cathode

too hard to indent small deformation created in nano-inden-tation, remarkable pile-up around the indentation region has not been observed. As a result, the stress directionality has been estimated by dividing axial component of the residual stress resulted from FEM analysis into radial residual stress component. Subsequently, biaxial stress analyses 0.54 was used as the stress ratio.

4 Results and discussion

4.1 Estimation of residual stresses

Temperature history computed in the thermal analysis is used as thermal load to calculate the residual stresses. In the finite element method, residual stresses were obtained after the cooling of workpiece back down to the ambient reference temperature. Figure 3 represents the profiles of the residual stress in X direction (radial direction in the two dimension modeling) along the depth at the center of the simulated domain. These residual stresses are related to the pulse duration of 100 μs, voltage of 200 V, and pulse current of 4 A. Also, Fig. 4 shows the experimental results of residual stress in X direction obtained by nano-indentation method for the workpiece EDMed with the same machining setting. As shown in these figures, the maximum of measured tensile residual stress is 2040 MPa where there

is a minor overestimation of 50 MPa or 2.5 % in the data obtained by the FEM result. As it is clear, there is a good agreement between stress profiles obtained by FEM and experimental observations.

In cooling phase, the local hot region in the surface has a tendency for expansion while being restricted by the surrounding cold material which leads to the development of tensile residual stresses at the surface of workpiece. According to the experimental observations and FEM results, the maximum tensile stress is developed not on the machined surface but beneath this surface. This phenomenon could be explained by this fact that some level of tensile residual stresses, as shown in Fig. 5, is relieved through the formation of microcracks on the machined surface.

Furthermore, for both of profiles represented in Figs. 3 and 4, the tensile residual stress at the machined surface is followed by a compressive residual stress in a depth that provides the mechanical equilibrium of machined workpiece. The machined surface is saturated with carbon resulted from the dissolution of dielectric fluid in the plasma channel (Fig. 6) [28]. This leads to a higher level of remaining austenite in the surface of machined workpiece. The remaining austenite is protected to some extent by the presence of compressive residual stresses [29].

As it is shown in Fig. 3, the maximum of calculated tensile residual stress is 2150 MPa that is slightly higher than ultimate tensile strength of workpiece (1990 MPa). As
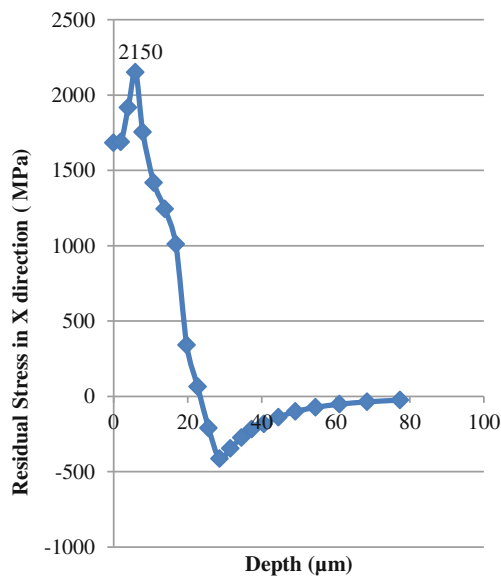

Fig. 3 FEM result of residual stress profile in X direction along the depth; pulse duration=100 μs, voltage=200 V, and pulse current=4A
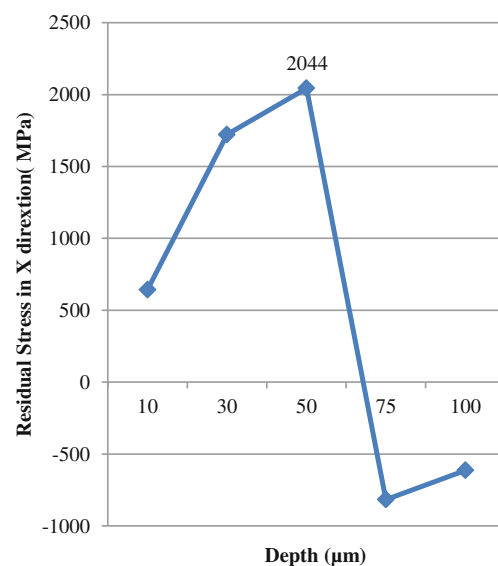

Fig. 4 The experimental result of residual stress in X direction along the depth; pulse duration=100 μs, voltage=200 V, and pulse current=4A
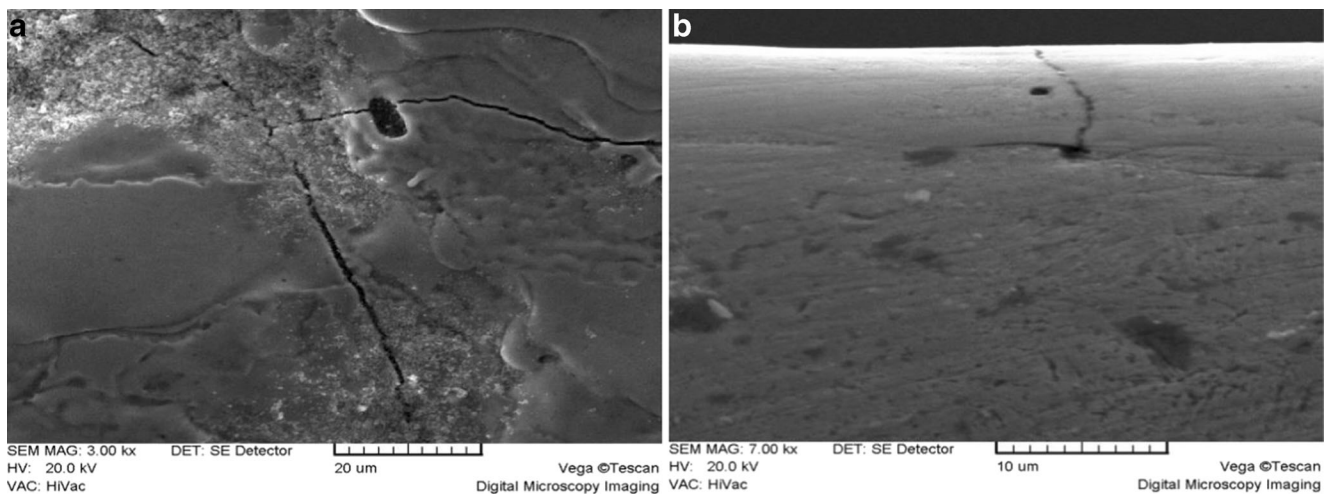
Fig. 5 **a** Surface micro-cracks and **b** cross-sectional view of EDMed surface. Pulse duration=100 μs, voltage=200 V, and pulse current=4A

can be seen from Table 2, the mechanical properties of material are temperature dependent. It is known that the temperature at the crater surface is very high and the stress values are limited by respective yield stress at each temperature. Thus, maximum tensile residual stress is observed in a depth where the complex interaction of thermal loading and temperature-dependant mechanical properties of the material occurs [30].

It can be seen from Figs. 3 and 4 that in FEM result, the maximum tensile residual stress is observed in a depth of 6 μm, and in experimental result, it occurs in a depth of 50 μm. In experimental result, the location of the peak stress is deeper and the peak width is wider than in the FEM result. These discrepancies can be related to the surface cracks on the machined workpiece (Fig. 5a, b) that are neglected in the FE simulation. Surface cracks cause the width of peak stress to be wider and also cause the location where the maximum tensile residual stress occurs to be deeper as they relieve some of the residual tensile stresses caused by the thermo-mechanical nature of EDM process.
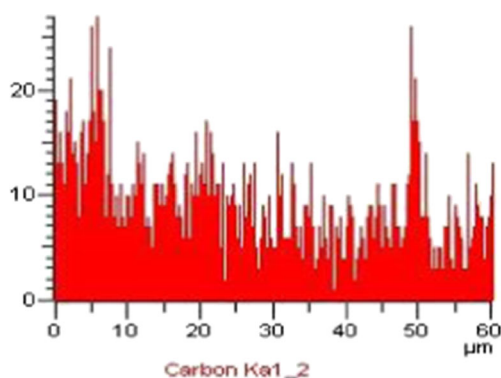
4.2 Influence of pulse current (*I*) and pulse duration (Ti) on residual stress distribution

In Fig. 7, distributions of the calculated residual stresses in X direction (radial direction in the two dimension modeling) along the depth for different pulse currents are shown. As can be seen, the maximum tensile residual stress values and the depth where these values are observed increase with the increase in the pulse current. In practice, this can cause the cracks formed on the EDMed surface to be deeper.

Figure 8 shows distributions of the calculated residual stresses in X direction (radial direction in the two dimension modeling) along the depth for different pulse durations. Similarly, the maximum tensile residual stress values and the depth where these values are observed increase with the increase in the pulse durations. Overall, it can be concluded that with the increase in discharge energy, the depth where the maximum tensile residual stress value is observed increases,
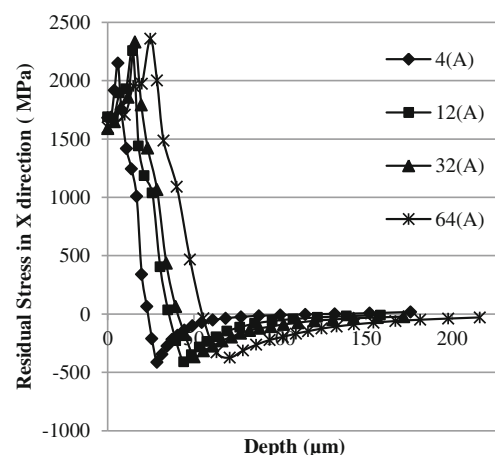

Fig. 6 Carbon insertion in the surface of sample that ED-machined in the pulse duration of 100 μs, voltage of 200 V, and pulse current of 4A

Fig. 7 FEM result of radial residual stresses variation along the depth of simulated domain for various pulse currents (Ti=100 μs)
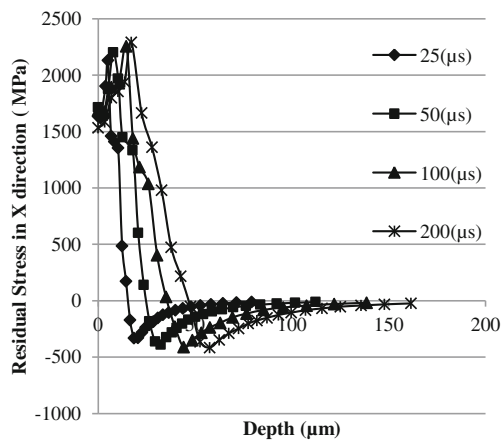
Fig. 8 FEM result of radial residual stresses variation along the depth of simulated domain for various pulse durations (I=12 A)

and this can lead to the creation of deeper surface cracks on EDMed surface. This phenomenon is in accordance with the findings of Ekmekci et al. [25].

It can be seen from Figs. 7 and 8 that the residual stress profile's form is independent from discharge energy. However, the width of peak increases with the increase in discharge energy.

change of work material due to austenite–martensite transformation into account.

- The maximum tensile residual stress occurs beneath the machined surface. This phenomenon is in accordance with previously published experimental findings and can be due to the stress relieving in the surface caused by the formation of surface micro-cracks and moreover the occurrence of carbon penetration in the surface layer which cause a slight compressive residual stresses in the workpiece surface.

- In the experimental result, the location of the peak stress is deeper and also the peak width is wider than in the calculated result. These discrepancies can be due to surface cracks that are neglected in FEM simulations.

- It can be seen that the residual stress profile form is independent from discharge energy, although with increase in pulse currents and pulse durations, the maximum tensile residual stress values and the depth where these values are observed increase.

- With the increase in discharge energy, the depth where the maximum tensile residual stress value is observed increases and this explains the creation of deeper surface cracks on EDMed surface when discharge energy increases.

5 Conclusions

In this paper, the results of a numerical model developed to predict the distribution of residual stresses from a single spark during EDM process have been represented. A sequentially coupled thermal, metallurgical, mechanical 3-D finite element model is introduced based on ABAQUS code. The time dependency of heat flux growth over the surface of part domain, heat dependency of physical properties of work material, and also effects of volume change due to austenite–martensite transformation on the final residual stress are considered into account during the simulations. The leading conclusions are as follows:

- The simulation results indicate that after one spark, tensile residual stresses developed around the crater and that these stresses can exceed ultimate strength of the workpiece material.

- The forms of both simulated and experimental residual stress profiles are quite similar although the pick of simulated one is slightly higher. This difference may be due to induced micro-cracks that cause to relief some of the surface residual stresses.

- The proximity of FE simulation results and experimental observations improves considerably by taking the time dependency of plasma channel growth, heat dependency of physical properties of part domain, and also volumetric

References

1. Yadav V, Jain VK, Dixit PM (2002) Thermal stresses due to electrical discharge machining. Int J Mach Tools Manuf 42:877–888
2. Soni PK, Gholley R (2007) Study and Analysis of Residual Stresses in Electrical-Discharge Machning (EDM), A Thesis in Partial Fulfillment of the Requirements for Degree of Bachelor of Technology in Mechanical Engineering, Department of Mechanical Engineering, National Institute of Technology, Rourkela
3. Lee JW (2003) Microstructural evaluation and phase transformation of recast layers in electrical discharge machined dual phase Fe-Mn-Al alloy. J Mater Sci 38(8):1679–1687
4. Mamalis AG, Vosniakos GC, Vaxevanidis NM (1987) Macroscopic and microscopic phenomena of electro-discharge machined steel surfaces: an experimental investigation. J Mech Work Technol 15: 335–356
5. DiBitonto D, Eubank PT, Patel MR, Barrufet MA (1989) Theoretical models of the electrical discharge machining process. I. A simple cathode erosion model. J Appl Phys 66:4095–4103
6. DiBitonto D, Eubank PT, Patel MR, Barrufet MA (1989) Theoretical models of the electrical discharge machining process. II. The Anode erosion model. J Appl Phys 73:7900–7909
7. Joshi SN, Pande SS (2010) Thermo-physical modeling of die-sinking EDM process. J Manuf Process 12:45–56
8. Tan PC, Yeo SH (2013) Simulation of surface integrity for nanopowder-mixed dielectric in micro electrical discharge machining. Metall Mater Trans B 44B:711–721
9. Shen Y, Liu Y, Zhang Y, Tan B, Ji R, Cai B, Zheng C (2014) Determining the energy distribution during electric discharge machining of Ti–6Al–4V. Int J Mach Tools Manuf 70:11–17

10. Ekmekci B (2007) Residual stresses and white layer in electric discharge machining (EDM). Appl Surf Sci 253:9234–9240

11. Yeo SH, Murali MS (2005) Process simulation and residual stress estimation of micro-electro discharge machining using finite element method. Jpn J Appl Phys 44:5254–5263

12. Das S, Klotz M, Klocke F (2003) EDM simulation: finite element-based calculation of deformation, microstructure and residual stresses. J Mater Process Technol 142:434–451

13. Rebelo JC, Kornmeier M, Batista AC, Dias AM (2002) Residual stress after EDM–FEM study and measurement results. J Mater Sci Forum 404–407:159–164

14. Ekmekci B (2002) Theoretical and experimental investigation of residual stresses in electrical discharge machining. Ph.D. Thesis. The Middle East Technical University

15. Ekmekci B, Tekkaya AE, Erden A (2006) A semi-empirical approach for residual stresses in electric discharge machining (EDM). Int J Mach Tools Manuf 46:858–868

16. Pradhan MK (2010) Modeling and simulation of thermal stress in electrical discharge machining process. Proc. Of the 4th International Conference on Advances in Mechanical Engineering. September 23–25. India, 360–364

17. Ikai T, Hashigushi K (1995) Heat input for crater formation in EDM. In Proceedings of international symposium for electro-machining-ISEM XI. EPFL. 163–170

18. Deng D (2009) FEM prediction of welding residuals stress and distortion in carbon steel considering phase transformation effects. Mater Des 30:359–366

19. Qi Shi MS (2002) Prediction of thermal distortion and thermal fatigue in shot sleeves. Ph.D. Thesis. The Ohio State University

20. Durand-Chare M (2003) Microstructure of steels and cast irons, ISBN 3-540-20963-8, Springer – Verlag Berline Heidelberg New York

21. Deng D, Murakawa H (2006) Prediction of welding residual stress in multi-pass butt welded modified 9Cr–1Mo steel pipe considering phase transformation effect. Comput Mater Sci 37:209–219

22. Dean D, Shoichi K, Hisashi S, Hidakazu M, Yukihiko H (2007) Numerical investigation on welding residual stress in 2.25Cr-1Mo steel pipes. Transit JWRI 36 (1)

23. Taylor CA, Wayne MF, Chiu WKS (2003) Residual stress measurement in thin carbon films by Raman spectroscopy and nanoindentation. Thin Solid Films 429:190–200

24. Dominique AU (2006) The effect of heat treatment atmosphere on hardening of surface region of H13 tool steel. Ph.D. Thesis. Auckland University of Technology

25. Ekmekci B, Elkoca O, Tekkaya AE, Erden A (2005) Residual stress state and hardness depth in electric discharge machining: de-ionized water as dielectric liquid. Taylor & Francis Inc. Mach Sci Technol 9:39–61

26. Choi MJ, Lee KW, Kim JY, Kim KH, Kwon D (2007) Application of instrumented technique to estimate strength and residual stress, HARDMEKO, Recent Advancement of Theory and Practice in Hardness Measurement, 19–21 November, Tsukuba, Japan

27. Lee YH, Kwon D (2004) Estimation of biaxial surface stress by instrumented indentation with sharp indenters. Acta Mater 52:1555–1563

28. Shabgard M, Nadimi Bavil Oliaei S, Seyedzavvar M, Najadebrahimi A (2011) Experimental investigation and 3D finite element prediction of the white layer thickness, heat affected zone, and surface roughness in EDM process. J Mech Sci Technol 25(12):3173–3183

29. Parish G (1999) Carburizing: Microstructures and Properties. ASM International, ISBN: 0-87170-666-0

30. Santiuste C, Thomsen OT, Frostig Y (2010) Thermo-mechanical load interactions in foam cored axi-symmetric sandwich circular plates—high-order and FE models. Compos Struct. doi:10.1016/j.compstruct.2010.09.005